第 34 卷第 3 期
2015 年 6 月

红 外 与 毫 米 波 学 报
J. Infrared Millim. Waves

Vol. 34, No. 3
June,2015

文章编号: 1001 - 9014(2015)03 - 0265 - 06

DOI:10.11972/j.issn.1001 - 9014.2015.03.002

A novel hybrid Freeman/eigenvalue decomposition with general scattering models

ZHANG Shuang[1*], WANG Shuang[1], JIAO Li-Cheng[1], CHEN Bo[1],
LIU Fang[1], MAO Sha-Sha[1], KE Xi-Zheng[2]

(1. Ministry of Education Key Lab. of Intelligent Perception and Image Understanding, Xidian University, Xi'an 710071, China;
2. School of Automation and Information Engineering, Xi'an University of Technology, Xi'an 710048, China)

Abstract: A novel hybrid Freeman/eigenvalue decomposition with general scattering models was proposed for polarimetric synthetic aperture radar (PolSAR) data. A unit matrix represents the volume scattering model, and eigenvectors corresponding to the two larger eigenvalues of the coherency matrix are used as the surface scattering model and double-bounce scattering model for non-reflection symmetry condition. There are three advantages in the proposed hybrid decomposition. Firstly, the surface and double-bounce scattering models are free from the reflection symmetry constraint which is more general and realistic for common media. Secondly, since the scattering powers of the proposed method are solved as linear combinations of the eigenvalues derived from the coherency matrix, they are all roll-invariant parameters. Thirdly, negative powers of surface scattering and double-bounce scattering are avoided with non-rotation of the coherency matrix. Fully PolSAR data on San Francisco are used in the experiments to prove the efficacy of the proposed hybrid decomposition.

Key words: polarimetric synthetic aperture radar, radar polarimetry, hybrid Freeman/eigenvalue decomposition, scattering model

PACS: 29.25.Pj, 84.40.Xb.

基于一般散射模型的 Hybrid Freeman/Eigenvalue 分解算法

张 爽[1*], 王 爽[1], 焦李成[1], 陈 博[1], 刘 芳[1], 毛莎莎[1], 柯熙政[2]
(1. 西安电子科技大学 智能感知与图像理解教育部重点实验室,陕西 西安 710071;
2. 西安理工大学,自动化与信息工程学院,陕西 西安 710048)

摘要:提出了一种新的基于一般散射模型的 hybrid Freeman/eigenvalue 分解算法,用于分析极化合成孔径雷达(PolSAR)数据。文中,单位矩阵作为体散射模型,相干矩阵的两个较大特征值对应的特征向量作为表面散射模型和二次散射模型,并且不需要反射对称条件。新算法有三个优点:第一,表面散射和二次散射不需要反射对称条件,更符合一般散射体的建模;第二,因为散射能量是相干矩阵特征值的线性组合,所以散射能量具有旋转不变性;第三,表面散射能量和二次散射能量避免了负值现象。在 San Francisco 地区的 AIRSAR 数据上进行了实验,证明了新算法的有效性。

关 键 词:极化合成孔径雷达;雷达极化;hybrid Freeman/eigenvalue 分解;散射模型

中图分类号:TP751.1 **文献标识码**:A

Introduction

Target decomposition is a useful tool to analyze and understand polarimetric synthetic aperture radar (PolSAR) data [1]. Currently, two kinds of decomposition techniques are commonly used. Eigenvector-based decompositions are derived from the eigenspace of the sec-

Received date: 2014 - 01 - 15, **revised date**: 2014 - 03 - 13 **收稿日期**:2014 - 01 - 15, **修回日期**:2014 - 03 - 13

Foundation items: Supported by the National Basic Research Program (973 Program) of China (2013CB329402) and the National Natural Science Foundation of China (61473215, 61472306, 61271302, 61272282, 61272176).

Biography: Zhang Shuang (1983-), female (Manzhu), Jinzhou, Ph. D. Research area involves PolSAR data interpretation and processing.

* **Corresponding author**: E-mail: shzhang_work@163.com

ond-order statistics matrix, for which the most popular approach is the Entropy/Alpha method developed by Cloude and Pottier[2]. Model-based decomposition methods, first proposed by Freeman and Durden[3], represent the polarimetric coherency matrix as the contributions of three or four physical scattering models. In Ref. [3], the covariance matrix was successfully decomposed into three components, surface scattering, double-bounce scattering and volume scattering, using the well-known reflection symmetry condition to analyze the natural distributed targets of the PolSAR data. Because of their simplicity and ease of implementation, Freeman-Durden decomposition (FDD) and later improved versions[4-14] have been widely used in PolSAR image applications[15-18].

A difficulty with FDD is that, under reflection symmetry condition, the cross-polarized component only contributes to the volume scattering model. This leads to an overestimation of the volume scattering power, often erroneously estimating it as larger than the total power. The method can then result in a number of negative surface and double-bounce scattering powers, especially in the presence of urban blocks or other man-made structures. In order to overcome this shortcoming, various improved model-based decomposition schemes[4-14] have been proposed. These improved decomposition methods are mainly categorized into three major groups. The first group improves the scattering power decomposition with an extended or modified scattering model[4-7]. The second group [8-9] are based on the deorientation theory [19]. In the third group, a combination of a modified scattering model and orientation angle compensation is used [10-14].

Many extended or improved scattering models have been proposed to reduce the number of negative surface and double-bounce scattering powers. Yamaguchi *et al.* [4] added the helix scattering model as the forth component to share the cross-polarized power, then obtained fewer negative values. Freeman [5] fitted a two-component scattering model and demonstrated the efficiency of separating the double-bounce scattering from volume scattering on tropical rain forest and temperate forest PolSAR data. Arii *et al.* [6] extended an adaptive model-based decomposition technique and iteratively estimated both the average orientation angle and the randomness degree for canopy scattering. Various modified three or four-component scattering power decompositions are analyzed with respect to the accurate estimation of volume scattering models in Ref. [7].

Based on deorientation theory [19], Yamaguchi *et al.* [8] rotated the coherency matrix to improve the four-component scattering power decomposition[4]. Lee *et al.* [9] analyzed the effect of orientation angle compensation on every element of the coherency matrix. This category considers that the overestimation of the volume scattering power is due to the shifted polarization orientation from sloped surfaces, oriented city blocks or other man-made media, and leads to power shifting from co-polarized term to cross-polarized term in the coherency matrix.

Deorientation theory and modified scattering models have been both considered. An *et al.* [10] decomposed the PolSAR data into three components with rotation of the coherency matrix[19], in which the unit matrix is used as the volume scattering model. Sato *et al.* [11] extended the volume scattering model suited for vegetation and dihedral structures which can well discriminate oriented buildings from vegetation areas. Two unitary transformations are used on the coherency matrix in Ref. [12], and the elements of the coherency matrix are all used in the scattering power decomposition. In order to reduce the number of unknowns, surface and double-bounce scattering models are set to be orthogonal by S. R. Cloude[13]. The scattering powers after the orientation angle compensation are effective at avoiding negative values, resulting in the well-known hybrid Freeman/eigenvalue decomposition. Singh *et al.* [14] improved the original hybrid Freeman/eigenvalue decomposition by using different volume scattering models scattered from vegetation areas and oriented objects.

In this paper, an improved version of hybrid Freeman/eigenvalue decomposition with general surface and double-bounce scattering models is proposed for PolSAR data, and a unit matrix is used as the volume scattering model. Our proposed hybrid decomposition does not require the reflection symmetry condition, which is a more realistic assumption for manmade media. The proposed surface scattering and double-bounce scattering models are derived from the eigenspace of the coherency matrix. The eigenvector with scattering angle α less than $\pi/4$ is used to represent the surface scattering model, while whose scattering angle α greater than $\pi/4$ is used to denote the double-bounce scattering model. We show how the eigenspace of the coherency matrix enables the proposed hybrid decomposition, and solve the scattering powers as the linear combinations of eigenvalues, so that the scattering powers are not only nonnegative values, but also all roll-invariant parameters.

The rest of this paper is organized as follows. The proposed hybrid Freeman/eigenvalue decomposition is presented in Section 1. Results and discussion of experiments performed on PolSAR data of San Francisco are provided in Section 2 and the final section presents our conclusions.

1 Proposed hybrid Freeman/ eigenvalue decomposition

For monostatic PolSAR system on $\{H, V\}$ basis, if reciprocal condition holds, a pixel of single look PolSAR data is represented by a Pauli vector [20] as:

$$\vec{k}_p = \frac{1}{\sqrt{2}}[S_{HH} + S_{VV} \quad S_{HH} - S_{VV} \quad S_{HV}]^t \quad (1)$$

where the superscript t is the transposition operator, S_{HH}, S_{VV}, and S_{HV} are the elements of the scattering matrix. For a multi-look PolSAR image, the ensemble average of the coherency matrix is given as a 3×3 positive semidefinite Hermitian matrix[20]:

$$\langle [T] \rangle = \langle \vec{k}_p \cdot \vec{k}_p^{*t} \rangle = \begin{bmatrix} T_{11} & T_{12} & T_{13} \\ T_{12}^* & T_{22} & T_{23} \\ T_{13}^* & T_{23}^* & T_{33} \end{bmatrix} \quad (2)$$

where the superscript $*$ is the complex conjugation operator, and $\langle \cdot \rangle$ denotes the ensemble average processor in a boxcar window.

The measured coherency matrix is decomposed into

three components, surface scattering, double-bounce scattering, and volume scattering as:

$$\langle [T] \rangle = m_s T_s + m_d T_d + m_v T_v \quad . \quad (3)$$

The original hybrid Freeman/eigenvalue decomposition was proposed by S. R. Cloude[13]. To improve the accuracy of the required parameter extraction, Singh *et al*. [14] improved the hybrid Freeman/eigenvalue decomposition technique with an extended volume scattering model, which can well discriminate oriented objects from vegetated or forested areas. In these papers, the reflection symmetry condition (i.e., $\langle S_{HH} S_{HV}^* \rangle \approx \langle S_{VV} S_{HV}^* \rangle \approx 0$) holds, but on city blocks or urban areas, since the orientation angle of manmade structures may not always be aligned with the radar line of sight, the reflection symmetry condition cannot hold (i.e., $\langle S_{HH} S_{HV}^* \rangle \neq \langle S_{VV} S_{HV}^* \rangle \neq 0$).

The average coherency matrix of a multi-look PolSAR image is decomposed [2] as:

$$\langle [T] \rangle = U \cdot \begin{bmatrix} \lambda_1 & 0 & 0 \\ 0 & \lambda_2 & 0 \\ 0 & 0 & \lambda_3 \end{bmatrix} \cdot U^{*t} \quad , \quad (4)$$

where λ_1, λ_2 and λ_3 are the eigenvalues of the coherency matrix with $\lambda_1 \geqslant \lambda_2 \geqslant \lambda_3 \geqslant 0$. U consists of the corresponding eigenvectors k_1, k_2, and k_3 [2] as:

$$U = [k_1 \quad k_2 \quad k_3] = \begin{bmatrix} \cos\alpha_1 & \cos\alpha_2 & \cos\alpha_3 \\ \sin\alpha_1 \cos\beta_1 e^{j\gamma_1} & \sin\alpha_2 \cos\beta_2 e^{j\gamma_2} & \sin\alpha_3 \cos\beta_3 e^{j\gamma_3} \\ \sin\alpha_1 \sin\beta_1 e^{j\delta_1} & \sin\alpha_2 \sin\beta_2 e^{j\delta_2} & \sin\alpha_3 \sin\beta_3 e^{j\delta_3} \end{bmatrix} . \quad (5)$$

The coherency matrix $\langle [T] \rangle$ is seen as an average target generated by a three-level Bernoulli statistical model. The eigenvectors k_1, k_2, and k_3 denote three different targets while the eigenvalues imply the corresponding amplitudes [21]. The physical meanings of the specific targets are defined as: α_i ($0 \leqslant \alpha_i \leqslant \pi/2$, $i = 1, 2, 3$) implies the scattering mechanisms; β_i ($-\pi/2 \leqslant \beta_i \leqslant \pi/2$) is the orientation angle; δ_i and γ_i are the phase angles. Among these parameters, α is the most important one. If $\alpha = 0$, the target is a pure surface scatter; if $\alpha = \frac{\pi}{2}$, the target is a dihedral scatter. Based on these, the scattering eigenvector with $0 \leqslant \alpha_s \leqslant \frac{\pi}{4}$ is defined in Eq. (6) [2] as surface targets, and this case typically occurs on surfaces such as bare soil or ocean. In contrast, the scattering eigenvector with $\frac{\pi}{4} < \alpha_d \leqslant \frac{\pi}{2}$ as defined in Eq. (7) [2] implies a double-bounce scattering target, which typically occurs on urban areas or cities, due to the wall-ground structures.

$$k_s = \begin{bmatrix} \cos\alpha_s \\ \sin\alpha_s \cos\beta_s e^{j\gamma_s} \\ \sin\alpha_s \sin\beta_s e^{j\delta_s} \end{bmatrix}, 0 \leqslant \alpha_s \leqslant \frac{\pi}{4} \quad , \quad (6)$$

$$k_d = \begin{bmatrix} \cos\alpha_d \\ \sin\alpha_d \cos\beta_d e^{j\gamma_d} \\ \sin\alpha_d \sin\beta_d e^{j\delta_d} \end{bmatrix}, \frac{\pi}{4} < \alpha_d \leqslant \frac{\pi}{2} \quad . (7)$$

Because of $0 \leqslant \alpha_s \leqslant \frac{\pi}{4}$ in (6), and $\frac{\pi}{4} < \alpha_d \leqslant \frac{\pi}{2}$ in Eq. (7), the condition $\langle S_{HH} S_{HV}^* \rangle \neq \langle S_{VV} S_{HV}^* \rangle \neq 0$ holds. We can draw a conclusion that the scattering models are presented without the assumption of reflection symmetry in the proposed hybrid decomposition.

We define the surface scattering model and double-boule scattering model as Eqs. (8) and (9) whose rank is equal to 1.

$$T_s = k_s * k_s^{*t} = \begin{bmatrix} \cos\alpha_s \\ \sin\alpha_s \cos\beta_s e^{j\gamma_s} \\ \sin\alpha_s \sin\beta_s e^{j\delta_s} \end{bmatrix} [\cos\alpha_s \quad \sin\alpha_s \cos\beta_s e^{-j\gamma_s} \quad \sin\alpha_s \sin\beta_s e^{-j\delta_s}]$$

$$= \begin{bmatrix} \cos^2\alpha_s & \cos\alpha_s \sin\alpha_s \cos\beta_s e^{-j\gamma_s} & \cos\alpha_s \sin\alpha_s \sin\beta_s e^{-j\delta_s} \\ \cos\alpha_s \sin\alpha_s \cos\beta_s e^{j\gamma_s} & \sin^2\alpha_s \cos^2\beta_s & \sin^2\alpha_s \sin\beta_s \cos\beta_s e^{-j(\delta_s - \gamma_s)} \\ \cos\alpha_s \sin\alpha_s \sin\beta_s e^{j\delta_s} & \sin^2\alpha_s \sin\beta_s \cos\beta_s e^{j(\delta_s - \gamma_s)} & \sin^2\alpha_s \sin^2\beta_s \end{bmatrix} \quad , \quad (8)$$

$$with \qquad 0 \leqslant \alpha_s \leqslant \frac{\pi}{4}$$

$$T_d = k_d * k_d^{*t} = \begin{bmatrix} \cos\alpha_d \\ \sin\alpha_d \cos\beta_d e^{j\gamma_d} \\ \sin\alpha_d \sin\beta_d e^{j\delta_d} \end{bmatrix} [\cos\alpha_d \quad \sin\alpha_d \cos\beta_d e^{-j\gamma_d} \quad \sin\alpha_d \sin\beta_d e^{-j\delta_d}]$$

$$= \begin{bmatrix} \cos^2\alpha_d & \cos\alpha_d \sin\alpha_d \cos\beta_d e^{-j\gamma_d} & \cos\alpha_d \sin\alpha_d \sin\beta_d e^{-j\delta_d} \\ \cos\alpha_d \sin\alpha_d \cos\beta_d e^{j\gamma_d} & \sin^2\alpha_d \cos^2\beta_d & \sin^2\alpha_d \sin\beta_d \cos\beta_d e^{-j(\delta_d - \gamma_d)} \\ \cos\alpha_d \sin\alpha_d \sin\beta_d e^{j\delta_d} & \sin^2\alpha_d \sin\beta_d \cos\beta_d e^{j(\delta_d - \gamma_d)} & \sin^2\alpha_d \sin^2\beta_d \end{bmatrix} \quad . \quad (9)$$

$$with \qquad \frac{\pi}{4} < \alpha_d \leqslant \frac{\pi}{2}$$

The volume scattering model is defined as a unit diagonal matrix whose rank is equal to 3 as Eq. (10). A related form of the volume scattering model was proposed by An *et al* [10] However, our volume scattering model is different from Ref. [10], in that it is derived from the eigenspace of the coherency matrix. In our method, an eigenvector denotes a target type, and the corresponding eigenvalue is the magnitude, so that the observed coherency matrix can be composed of contributions from three different types of target. The volume scattering model is designed as a random distributed target, diffused from three different scattering mechanisms (eigenvectors) with equal magnitudes (eigenvalues), which can be written as Eq. (11).

$$T_v = \frac{1}{3} \begin{bmatrix} 1 & 0 & 0 \\ 0 & 1 & 0 \\ 0 & 0 & 1 \end{bmatrix} \quad , \quad (10)$$

$$\frac{1}{3}k_1k_1^{*t}+\frac{1}{3}k_2k_2^{*t}+\frac{1}{3}k_3k_3^{*t}=\frac{1}{3}\begin{bmatrix}1&0&0\\0&1&0\\0&0&1\end{bmatrix}=T_v \quad .(11)$$

We substitute the surface scattering model Eq. (8), double-bounce scattering model Eq. (9), and volume scattering model Eq. (10) into Eq. (3), and expand the coherency matrix into eigenspace:

$$\begin{aligned}\langle[T]\rangle &= m_sT_s+m_dT_d+m_vT_v\\ &=\lambda_1k_1k_1^{*t}+\lambda_2k_2k_2^{*t}+\lambda_3k_3k_3^{*t}\\ &=(\lambda_1-\lambda_3)k_1k_1^{*t}+(\lambda_2-\lambda_3)k_2k_2^{*t}\\ &+3\lambda_3\left(\frac{1}{3}k_1k_1^{*t}+\frac{1}{3}k_2k_2^{*t}+\frac{1}{3}k_3k_3^{*t}\right)\\ &=(\lambda_1-\lambda_3)k_1k_1^{*t}+(\lambda_2-\lambda_3)k_2k_2^{*t}+3\lambda_3T_v \quad .(12)\end{aligned}$$

From Eq. (12), the volume scattering power is solved as:

$$m_v=3\lambda_3 \quad .(13)$$

The surface scattering power m_s and double-bounce scattering power m_d are the eigenvalues of T_{SD}, which is shown in Eq. (14). Thus, when $\alpha_1\leqslant\frac{\pi}{4}$, we obtain $\alpha_s=\alpha_1$, $T_s=k_1k_1^{*t}$, $\alpha_d=\alpha_2$ and $T_d=k_2k_2^{*t}$, then the scattering powers m_s and m_d are solved as (26). Similarly, when $\alpha_2\leqslant\frac{\pi}{4}$, we obtain $\alpha_s=\alpha_2$, $T_s=k_2k_2^{*t}$, $\alpha_d=\alpha_1$ and $T_d=k_1k_1^{*t}$, and then the scattering powers, m_s and m_d, are given as Eqs. (15) and (16).

$$\begin{aligned}T_{SD}&=\langle[T]\rangle-m_vT_v\\ &=m_sT_s+m_dT_d\\ &=(\lambda_1-\lambda_3)k_1k_1^{*t}+(\lambda_2-\lambda_3)k_2k_2^{*t}\end{aligned} \quad ,(14)$$

$$\begin{aligned}m_s&=\lambda_1-\lambda_3\\ m_d&=\lambda_2-\lambda_3\end{aligned}\quad \text{if } \alpha_1\leqslant\frac{\pi}{4} \quad ,(15)$$

$$\begin{aligned}m_s&=\lambda_2-\lambda_3\\ m_d&=\lambda_1-\lambda_3\end{aligned}\quad \text{if } \alpha_2\leqslant\frac{\pi}{4} \quad .(16)$$

The number of negative scattering powers is an important factor in determining the efficiency of the scattering power decomposition. By using Eqs. (13), (15), (16), and $\lambda_1\geqslant\lambda_2\geqslant\lambda_3\geqslant0$, negative values of the scattering powers m_s, m_d, and m_v are avoided. Additionally, m_s, m_d, and m_v are the linear combinations of $\{\lambda_1, \lambda_2, \lambda_3\}$, and $\{\lambda_1, \lambda_2, \lambda_3\}$ are roll-invariant parameters, so the scattering powers m_s, m_d, and m_v are also all roll-invariant.

2 Experiments and discussions

To demonstrate the validity of the proposed hybrid Freeman/eigenvalue decomposition, the experiments were conducted on the four-look L-band fully PolSAR data of San Francisco. The data were acquired by NASA/JPL ARISAR. The spatial resolution is about 10 m × 10 m and the radar incidence angles span from 5° to 60°. The PolSAR data-set is publicly available and can be downloaded from Ref. [22]. The PolSAR data-set used in these experiments has 700 × 600 pixels. The original image is shown in Fig. 1, with diagonal components of the coherency matrix: ||HH − VV|| for red, 2||HV|| for green and ||HH + VV|| for blue. The selected zones, indicated by red rectangles, were used in the experiments, and represent ocean areas, city blocks and forests terrain. To remove noise, a sigma filter [23] with sigma = 0.9, window of target = 3, window of filter = 9 was used before decomposition.

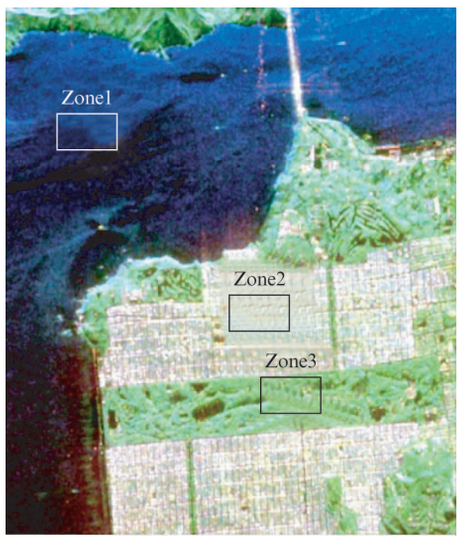

Fig. 1 AIRSAR image of San Francisco (||HH − VV|| in red, 2||HV|| in green, ||HH + VV|| in blue)
图 1 San Francisco 的 AIRSAR 图像(||HH − VV||, 2||HV||, ||HH + VV||分别作为 R,G,B 三通道)

In order to assess the property non-reflection symmetry, i.e. $\langle S_{HH}S_{HV}^*\rangle\neq\langle S_{VV}S_{HV}^*\rangle\neq0$. This property can be considered as valid as long as

$$\omega=\frac{2\left(|\langle S_{HH}S_{HV}^*\rangle|+|\langle S_{VV}S_{HV}^*\rangle|\right)}{[|S_{HH}|^2]+[|S_{VV}|^2]+2[|S_{HV}|^2]}\gg0 \quad .(17)$$

The range of the non-reflection symmetry parameter ω is $0\leqslant\omega\leqslant1$. If $\omega\approx0$, the reflection symmetry holds; if $\omega\gg0$, the data set are free from the reflection symmetry. In Table 1, we show the mean values of ω in the three selected zones.

Table 1 Means of ω in the selected zones
表 1 被选取的小区域中非反射对称参数 ω 的均值

	Zone 1	Zone 2	Zone 3
mean_ω	0.130 9	0.299 1	0.109 6

The mean values of ω in the three zones are up to 0.299 1, which implies that the reflection symmetry does not hold.

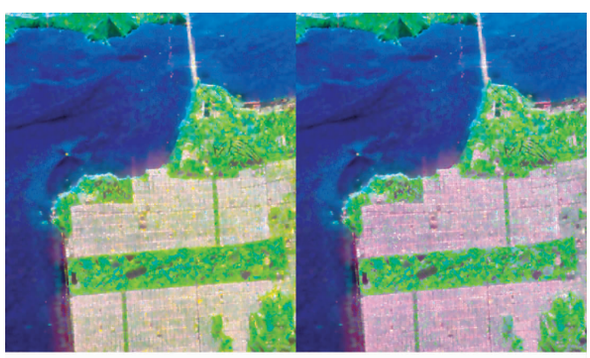

(a) (b)

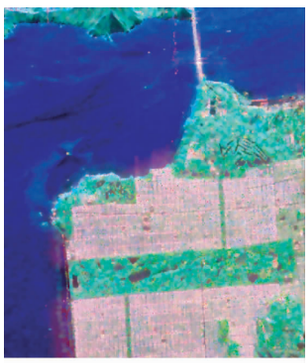

(c)

Fig. 2　Decompositions of AIRSAR data on San Francisco with m_s for blue, m_d for red, m_v for green. (a) Original hybrid Freeman/eigenvalue decomposition, (b) Hybrid Freeman/eigenvalue decomposition with extended volume scattering model, (c) Proposed hybrid Freeman/eigenvalue decomposition

图 2　San Francisco 地区 AIRSAR 数据的分解,m_s, m_d, 和 m_v 分别表示 R,G,B 彩色三通道. (a)原始的 hybrid Freeman/eigenvalue 分解,(b)基于扩展的体散射模型的 hybrid Freeman/eigenvalue 分解,(c)本文算法

In order to show the efficiency of the proposed hybrid Freeman/eigenvalue decomposition, we compare its performance against both the original hybrid Freeman/eigenvalue decomposition [13] (HFED 1) and also the hybrid Freeman/eigenvalue decomposition with extended volume scattering model [14] (HFED 2). The AIRSAR data are decomposed into three components: surface scattering power m_s (blue), double-bounce scattering power m_d (red), and volume scattering power m_v (green) shown in Fig. 2.

Three main types of terrain, i.e., ocean areas, city blocks, and forests are observed in Fig. 1. It is well known, that the dominant scattering powers of these types of ground cover are surface scattering power, double-bounce scattering power and volume scattering power, respectively. From Fig. 2(a) ~ (c), we can see that the results from three compared techniques all satisfy this rule. For further analysis, three zones are selected and marked by red rectangles (see Fig. 1), labeled Zone 1, Zone 2 and Zone 3. Each Zone is 50×80 pixels and the types of ground truth for Zone 1, Zone 2, and Zone 3 are ocean areas, city blocks, and forests, respectively. The mean values of surface scattering power in Zone 1, double-bounce scattering power in Zone 2, and volume scattering power in Zone 3 are represented by $mean\_m_s$, $mean\_m_d$, and $mean\_m_v$, respectively, and they are listed in Table 2.

The scattering powers m_s, m_d, and m_v are normalized by the total powers (i.e., $m_s + m_d + m_v$). In Zone 1, it can be seen that $mean\_m_s$ given by the proposed method is 0.950 1 which is about 6.9% higher than the other two decompositions. Because of the complexity of the man-made structures, the double-bounce scattering power is a critical feature for city blocks. In Zone 2, the result of the proposed hybrid decomposition also outperforms the other two methods. Specifically, $mean\_m_d$ by the proposed method is 0.508 4, which is 6.5% and 3.8% higher than the mean values of HFED 1 and HFED 2 respectively. However, in Zone 3, $mean\_m_v$ given by HFED 1 is the largest. In the proposed hybrid Freeman/eigenvalue decomposition, because the reflection symmetry condition does not hold, the cross-polarized power contributes to all three scattering models, which leads to the surface scattering power and the double-bounce scattering power having higher values than those generated by the current hybrid Freeman/eigenvalue decomposition techniques.

Table 2　Means of dominated scattering powers in the selected zones

表 2　被选取的小区域中主导散射能量的均值

	$mean\_m_s$ (Zone 1)	$mean\_m_d$ (Zone 2)	$mean\_m_v$ (Zone 3)
HFED 1	0.888 7	0.477 5	0.827 7
HFED 2	0.888 7	0.490 0	0.786 9
Proposed method	0.950 1	0.508 4	0.646 4

To evaluate the impact of noise on the proposed hybrid Freeman/eigenvalue decomposition, the AIRSAR data were processed by a set of mean filters whose window sizes span from 3×3 to 15×15. For simplicity, we only show the scattering powers of the three selected zones in Fig. 1. The mean values of surface scattering powers in Zone 1, double-bounce scattering powers in Zone 2, and volume scattering powers in Zone 3 are listed in Table 3. It can be seen that $mean\_m_d$ in Zone 2 and $mean\_m_v$ in Zone 3 are increased by 7.49% and 6.63%, respectively, with the window size from 3×3 to 15×15, however, $mean\_m_s$ in Zone 1 is decreased by just 0.03% which we suggest is negligible. The impact of noise on Zone 3 (ground truth is forests and the primary scattering power is m_v) and Zone 2 (ground truth is city blocks and the primary scattering power is m_d) is strong, however, the impact on Zone 1 (ground truth is ocean areas and the primary scattering power is m_s) is weak, since the ground cover is more complicated and thus the noise is stronger. Therefore with bigger window sizes, the effect of denoising on Zone 3 and Zone 2 is better. For Zone 1, a mean filter with a large window reduces the surface scattering power by a small range, because the third eigenvalue of the coherency matrix becomes large when the window size increases. The mean values in Table 3 are all bigger than 0.5, therefore, even though noise may impact the proposed method by decreasing the primary scattering power, it still does not prevent a correct terrain classification.

In the basis of the proposed hybrid decomposition, α_s and α_d are the important parameters. But the basis changes from pixel to pixel even in a uniform area, which happens on both the proposed hybrid decomposition, and also the compared hybrid Freeman/eigenvalue decomposition. In Table 4, we list the mean values ($mean\_\alpha_{s,d}$) and standard deviations ($std\_\alpha_{s,d}$) of two parameters in the three selected zones. On Zone 1 and Zone 3, std_α_s and std_α_d are the lowest parameters obtained by the proposed hybrid decomposition. In contrast, for Zone 2, std_α_s and std_α_d given by HFED 1 are the best, followed by the results of the proposed hybrid decomposi-

tion, with HFED 2 performing the worst. From Table 4, we can conclude that, in uniform areas, α_s and α_d, derived from the proposed hybrid decomposition method, lie in acceptable ranges.

Table 3 Means of the scattering powers under various window sizes

表 3 散射能量在不同滤波窗口下的均值

	$mean\_m_s$ (Zone 1)	$mean\_m_d$ (Zone 2)	$mean\_m_v$ (Zone 3)
No filter	0.950 1	0.508 4	0.646 4
3×3 mean filter	0.950 1	0.512 7	0.668 5
5×5 mean filter	0.950 1	0.529 2	0.680 5
7×7 mean filter	0.950 0	0.539 9	0.690 2
9×9 mean filter	0.950 0	0.545 8	0.696 7
11×11 mean filter	0.949 9	0.549 5	0.703 2
13×13 mean filter	0.949 9	0.550 5	0.708 6
15×15 mean filter	0.949 8	0.551 1	0.712 8

Table 4 Means and standard deviations of α_s and α_d ($mean\_\alpha \pm std\_\alpha$)

表 4 α_s 和 α_d 的均值和标准差(均值±标准差)

		Zone 1	Zone 2	Zone 3
α_s (degree)	HFED 1	17.105 2±2.456 4	8.257 5±7.696 8	22.699 5±13.917 0
	HFED 2	17.105 2±2.456 4	19.910 2±12.572 2	23.124 2±13.642 7
	Proposed Method	16.534 8±1.731 3	20.723 4±10.109 4	28.209 0±8.669 1
α_d (degree)	HFED 1	72.894 8±2.456 4	81.742 5±7.696 8	67.300 5±13.917 0
	HFED 2	72.894 8±2.456 4	70.089 8±12.572 2	66.875 8±13.642 7
	Proposed Method	73.967 0±1.772 8	70.324 0±10.878 1	64.056 7±8.669 1

3 Conclusions

In this paper, a novel version of hybrid Freeman/eigenvalue decomposition with general scattering models has been presented for polarimetric SAR data analysis. Three improvements can be included in the proposed method. Experimental results showed that the proposed method works better than the current hybrid decompositions. In addition, neither the original Freeman/eigenvalue decomposition nor the improved version utilized the full polarimetric information, while the proposed hybrid decomposition uses the nine parameters of the coherency matrix.

References

[1] Cloude S. R. Pottier E. A review of target decomposition theorems in radar polarimetry [J]. *IEEE Transactions on Geoscience and Remote Sensing*, 1996, **34**(2): 498-518.

[2] Cloude S. R Pottier E. An entropy based classification scheme for land applications of polarimetric SAR [J]. *IEEE Transactions on Geoscience and Remote Sensing*, 1997, **35**(1): 68-78.

[3] Freeman A., Durden S. L. A three-component scattering model for polarimetric SAR data [J]. *IEEE Transactions on Geoscience and Remote Sensing*, 1998, **36**(3): 963-973.

[4] Yamaguchi Y., Moriyama T., Ishido M., *et al*. Four-component scattering model for polarimetric SAR image decomposition [J]. *IEEE Transactions on Geoscience and Remote Sensing*, 2005, **43**(8): 1699-1706.

[5] Freeman A. Fitting a Two-Component Scattering Model to Polarimetric SAR Data from Forests [J]. *IEEE Transactions on Geoscience and Remote Sensing*, 2007, **45**(8): 2583-2592.

[6] Arii M., Zyl J. J. van, Kim Y. J. Adaptive model-based decomposition of polarimetric SAR covariance matrices [J]. *IEEE Transactions on Geoscience and Remote Sensing*, 2011, **49**(3): 1104-1113.

[7] Antropov O., Rauste Y. Häme T. Volume scattering modeling in PolSAR decomposition: study of ALOS PALSAR data over Boreal forest [J]. *IEEE Transactions on Geoscience and Remote Sensing*, 2011, **49**(10): 3838-3848.

[8] Yamaguchi Y., Sato A., Boerner W. M. *et al*. Four-component scattering power decomposition with rotation of coherency matrix [J]. *IEEE Transactions on Geoscience and Remote Sensing*, 2011, **49**(6): 2251-2258.

[9] Lee J. S., Ainsworth T. L. The effect of orientation angle compensation on coherency matrix and polarimetric target decompositions [J]. *IEEE Transactions on Geoscience and Remote Sensing*, 2011, **49**(1): 53-64.

[10] An W., Cui Y., Yang J. Three-component model-based decomposition for Polarimetric SAR data [J]. *IEEE Transactions on Geoscience and Remote Sensing*, 2010, **48**(6): 2732-2739.

[11] Sato A., Yamaguchi Y., Singh G. *et al*. Four-component scattering power decomposition with extended volume scattering model [J]. *IEEE Transactions on Geoscience and Remote Sensing*, 2012, **9**(2): 166-170.

[12] Singh G., Yamaguchi Y. Park S. E. General four-component scattering power decomposition using unitary transformation [J]. *IEEE Transactions on Geoscience and Remote Sensing*, 2013, **51**(5): 3014-3022.

[13] Cloude S. R. Polarisation: Applications in Remote Sensing [M]. *London, U. K.: Oxford Univ. Press*, 2009.

[14] Singh G., Yamaguchi Y., Park S. E., *et al*. Hybrid Freeman/Eigenvalue decomposition method with extended volume scattering model [J]. *IEEE Geoscience Remote Sensing Letters*, 2013, **10**(1): 81-83.

[15] Lee J. S., Grunes M. R., Pottier E., *et al*. Unsupervised terrain classification preserving scattering characteristics [J]. *IEEE Transactions on Geoscience and Remote Sensing*, 2004, **42**(4): 722-731.

[16] Berman J. D. B., Sanchez J. M. L. Applying the Freeman-Durden Decomposition Concept to Polarimetric SAR Interferometry [J]. *IEEE Transactions on Geoscience and Remote Sensing*, 2010, **48**(1): 466-479.

[17] Sharma J. J., Hajnsek I., Papathanassiou K. P., Polarimetric decomposition over Glacier ice using long-wavelength airborne PolSAR [J]. *IEEE Transactions on Geoscience and Remote Sensing*, 2011, **49**(1): 519-535.

[18] Neumann M., Ferro-Famil L., Reigber A. Improvement of vegetation parameter retrieval from polarimetric SAR interferometry using a simple polarimetric scattering model. [J]. *POLinSAR* 2009, *Rome*, *Italy*, *Jan*. 2009.

[19] Xu F., Jin Y. Q. Deorientation theory of polarimetric scattering targets and application to terrain surface classification [J]. *IEEE Transactions on Geoscience and Remote Sensing*, 2005, **43**(10): 2351-2364.

[20] Cloude, S. R., Group theory and polarization algebra [J] *OPTIK*, 1986, **75**(1):26-36.

[21] Lee J. S., Pottier E. Polarimetric Radar Imaging: From Basics to Applications [M]. *Boca Raton*, FL: CRC Press, 2009.

[22] http://earth.eo.esa.int/polsarpro/datasets.html[EB OL].

[23] Lee J S. Improved sigma filter for speckle filtering of SAR imagery [J]. *IEEE Transactions on Geoscience and Remote Sensing*, 2009, **47**(1): 202-213.